ADVANCED MATERIALS

Supporting Information

for *Adv. Mater.*, DOI: 10.1002/adma.202004560

Covalent Graphene-MOF Hybrids for High-Performance Asymmetric Supercapacitors

Kolleboyina Jayaramulu, Michael Horn, Andreas Schneemann, Haneesh Saini, Aristides Bakandritsos, Vaclav Ranc, Martin Petr, Vitalie Stavila, Chandrabhas Narayana, B#a#ej Scheibe, Št#pán Kment, Michal Otyepka, Nunzio Motta, Deepak Dubal,* Radek Zbo#il,* and Roland A. Fischer**

Supporting Information

Covalent Graphene-MOF Hybrids for High Performance Asymmetric Supercapacitors

Kolleboyina Jayaramulu* Michael Horn, Andreas Schneemann, Haneesh Saini, Aristides Bakandritsos, Vaclav Ranc, Martin Petr, Vitalie Stavila, Chandrabhas Narayana, Błażej Scheibe, Štěpán Kment, Michal Otyepka, Nunzio Motta, Deepak Dubal,* Radek Zboril,* and Roland A Fischer*

Experimental Section

1. Materials

All reagents and solvents were commercially available and used as supplied without further purification. $ZrCl_4$, 2-aminoterepthalic acid, 4-aminobenzoic acid, NaCN (p.a. ≥97%), graphite fluoride (>61 wt.% F, C1F1.1), were obtained from Sigma-Aldrich. Acetone (pure), ethanol (absolute) and potassium chloride were purchased from Penta. Amine free dimethylformamide (DMF), nitric acid (Analupure®, 65%) were obtained from Lach-Ner.

2. Methods

2.1. Synthesis of functional Graphene Acid (GA)

GA was prepared according to literature.[30] To prepare Graphene acid, the commercial Fluorinated graphene oxide (120 mg) is placed in a 25 mL round bottom glass flask with 15 mL of DMF and sonicated for 4h under nitrogen atmosphere. Subsequently, 800 mg sodium cyanide are added (NaCN) and the

mixture is heated at 130 °C with a condenser under stirring (500 rpm) for 24 h. The mixture was left to cool to room temperature, and an equal amount of acetone added. The materials were then separated by centrifugation and further purified by successive washing steps using DMF, dichloromethane, acetone, ethanol and water (all 4×). Afterwards the material was washed with hot (80 °C) DMF and water. During the final centrifugation steps with water, it was necessary to apply centrifugal forces of up to 25 000 rpm to isolate the product cyanographene. The cyanographene was transformed into graphene acid by mixing it with HNO_3 (65%) under stirring at room temperature. Afterwards the mixture was then heated at 100 °C and stirred (350 rpm) for 24 h. The final product was thoroughly washed with water to remove soluble impurities. It should be noted that, the stable aqueous suspensions of G-COOH were prepared by adjusting the pH of the purified suspension to ∼8.

2.2. Synthetic procedure for UiO-66-NH_2

Octahedral nano crystals of Uio66-NH_2 were prepared according to a slightly modified literature procedure. $ZrCl_4$ (0.233 g) and 2-aminoterepthalic acid (0.181 g)and 4-aminobenzoic acid (0.244 g) were mixed in 10 ml dimethylformamide (DMF) solvent in glass vial and dissolved by addition of 0.16 ml of hydrochloric acid (HcL). Later, the glass vial was tightly closed and placed in an oven at 120 °C for 2 days. After cooling to room temperature, the supernatant was decanted, and the pale-yellow precipitate was washed three times with DMF and three times with methanol. Methanol was decanted and replaced once per day during the course of three days and later it was removed under vacuum. The product was heated under vacuum to 150 °C for 5 h. The sample was cooled to room temperature and stored under ambient conditions.

2.3. Synthetic procedure for UiO-66

Octahedral nano crystals of UiO-66 were prepared according to a slightly modified literature procedure. $ZrCl_4$ (0.233 g), terephthalic acid (0.166 g) and 4-aminobenzoic acid (0.244 g) were mixed in 10 ml dimethylformamide (DMF) solvent in a glass vial and dissolved by addition of 0.16 ml of hydrochloric acid (HCl). Afterwards, the glass vial was tightly sealed and placed in an oven at 120 °C for 2 days. After cooling to room temperature, the supernatant was decanted, and the pale-yellow precipitate was washed three times with DMF and three times with methanol. Methanol was decanted and replaced

once per day during the course of three days and later it was removed under vacuum. The product was heated under vacuum to 150 °C for 5 h. The sample was cooled to room temperature and stored under ambient conditions.

2.4. Preparation of Noncovalent Hybrid MOF GA@Uio-66

A sample of 100 mg of GA was exfoliated in 10 mL of DMF solution for 30 minutes under sonication. To this GA suspension, $ZrCl_4$ (233 mg), 2-aminoterepthalic acid (166 mg), 4-aminobenzoic acid (244 mg) and 0.16 ml of HCl were added into a 25 ml glass vial. The resultant mixture was sonicated for 30 minutes. The resultant mixture was transferred to a 50 ml glass vial and placed in a 120 °C oven for 2 days. The obtained black gel was washed several times with methanol and dried under nitrogen atmosphere at 150 $^{\circ}$C.

2.5. Preparation of Covalent Hybrid MOF GA@Uio-66-NH_2

A sample of 100 mg of GA was exfoliated in 10 mL of DMF solution for 30 minutes under sonication. To this GA suspension, $ZrCl_4$ (0.233 g), 2-aminoterepthalic acid (0.181 g), 4-aminobenzoic acid (0.244 g) and 0.16 ml of HCl was added into a 25 ml glass vial. The resultant mixture was sonicated for 30 minutes. The resultant mixture was transferred to a 50 ml glass vial and placed in a 120 °C oven for 2 days. The obtained black gel was washed several times with methanol and dried under nitrogen atmosphere at 100 $^{\circ}$C.

2.6. Preparation of physical mixture of GA and UiO-66-NH_2 (denoted as GA/Uio-66-NH2)

A sample of as-synthesized GA (50 mg) and UiO-66-NH_2 nanocrystals (50 mg) were grounded in a mortar for 5 minutes. The obtained black color powder was activated under nitrogen atmosphere at 150 $^{\circ}$C to remove solvent molecules.

2.7. Synthesis of Mxene ($Ti_3C_2T_x$) nanosheets

The MXenes were synthesized by selective etching of aluminum from the Ti_3AlC_2 (purchased from Carbon, Ukraine) using minimally intensive layer delamination (MILD) method. Initially, 1 g of Ti_3AlC_2

powder was slowly added in the mixture of 1 g LiF and 20 ml of 6 M HCl for 24 h at 35 °C with continuous stirring. After the etching process, the solution was repeatedly washed with deionized water and centrifuged until neutral pH was reached. The resulting mixture was collected using vacuum-assisted filtration method and dried in a vacuum oven at 60 °C for 24 h to obtain multilayered powder. In the next step, 0.25 g $Ti_3C_2T_x$ powder was re-dispersed in 25 ml of deionized water and was bath sonicated for 1 h. The suspension was further centrifuged, and supernatant was collected, which contained few layered MXenes nanosheets. The suspension was finally filtered and dried in a vacuum oven.

3. Characterization

The synthesized materials were characterized by different techniques. X-ray diffraction (XRD) data of all samples were collected by a PANalytical X'Pert PRO instrument in Bragg-Brentano geometry with automatic divergence slits, position sensitive detector in continuous mode at room temperature using Cu-Kα radiation and a Ni filter. The morphology and porous nature was characterized through scanning electron microscopy (FESEM-FEI Nova-Nano SEM-600) and transmission electron microscopy (JEOL JEM-3010 with accelerating voltage at 300 kV). X-ray photoelectron spectroscopy (XPS) was performed on a PHI 5000 Versa Probe II scanning XPS microprobe from Physical Electronics, using X-ray radiation from an Al source equipped with a monochromator. Spectra were collected and evaluated with the MultiPak (ULVAC-PHI, Inc.) software. All binding energies were referenced to the C1s peak at 284.8 eV. The Raman spectra of the samples were collected with a DXR Raman instrument (Thermo Fisher Scientific, USA); laser wavelength: 633 nm, laser power on sample: 2mW, exposition time: 5s. 32 spectra were averaged at each spot to obtain one data point. N_2 Adsorption studies (77 K) were carried out using a MICROMERITICS analyzer. Prior to each measurement the samples were outgassed at 423 K under high vacuum on the activation port of the instrument for 12 hours. The gases (nitrogen, carbon dioxide, and argon) for adsorption studies were obtained from Chemixgases, India, and were 99.99% pure. In-situ Raman spectra were recorded using a custom-built Raman spectrometer with a HeNe red laser (632.8 nm) and 1800 lines/mm grating Laser power was 8 mW at the sample. Temperature dependent Raman studies were done using a Linkam THMS 600 heating–cooling stage. Typical accumulation time was 30 s for all the Raman studies. For gas adsorption Raman studies, activated powder graphene acid (GA), **GA@UiO-66-NH_2** was mounted on the Linkam stage, and heated to 80 °C and then cooled to room temperature (RT) after which the gases were purged. Temperature was monitored through the temperature controller attached to the Linkam stage. The gas pressure was regulated by the regulator

fixed at the inlet and was mostly kept constant around 1 atm. The Raman spectra obtained were smoothened using 5-point FFT, and baseline correction was done to remove the background

4. Electrode fabrication and electrochemical testing

Conducting carbon fabric (CF) was used as current collector, which was initially cleaned with de-ionized water and ethanol. The suspension of electrode materials (GA@UiO-66-NH_2 or $Ti_3C_2T_x$) were prepared by sonicating suitable amount (5 mg/ml) of powder samples. Finally, the colloidal solutions were sprayed pre-cleaned CF substrate and followed by drying at 60° C in vacuum oven. The mass loading on the CF substrate was controlled based on the composition of colloidal solution and number of layers.

Prior to assemble a full cell, GA@UiO-66-NH_2 and $Ti_3C_2T_x$ electrodes were tested in 1 M Na_2SO_4 electrolyte using 3-electrode configuration where the reference and counter electrodes were Ag/AgCl (saturated KCl) and platinum plate, respectively. A home-built Swagelok type cell was used with a Whatman glass fiber filter as the separator. In order to approach the highest cell voltage, the charges stored in positive and negative electrodes must be balanced by adjusting the mass loading of each of the active electrode materials. The capacitance of the GA@UiO-66-NH2 and $Ti_3C_2T_x$ electrodes were balanced to satisfy $Q_+ = Q_-$.

$$\frac{m_{MXene}}{m_{C-MOF}} = \frac{C_{C-MOF} \times E_{C-MOF}}{C_{MXene} \times E_{MXene}} = \frac{1}{1.5} \qquad (1)$$

The mass ratio of GA@UiO-66-NH_2:$Ti_3C_2T_x$ was maintained to ~ 1:1.5. Thus, the total mass loading of active material in both electrodes was 3.1 mg/cm^2.

The electrochemical performances of individual electrodes and final asymmetric cells such as cyclic voltammetry (CV) and galvanostatic charge/discharge (GCD) were conducted using a Biologic VMP300 electrochemical workstation.

Calculations: Specific capacitance (F/g) of electrode materials as well as device were calculated from the CD curves by integrating the discharge portion using the following equation:

$$C = \frac{I \cdot \int V \cdot dt}{m \cdot V^2} \qquad (2)$$

Where, I is current in A, V is potential/voltage window and m is mass of the active material. The specific energy (E, Wh/kg) and specific power (P, W/kg) of the device were obtained from the following equations:

$$E = \frac{1}{2\times 3.6} C\Delta V^2 \qquad (3)$$

$$P = \frac{3600\times E}{\Delta t} \qquad (4)$$

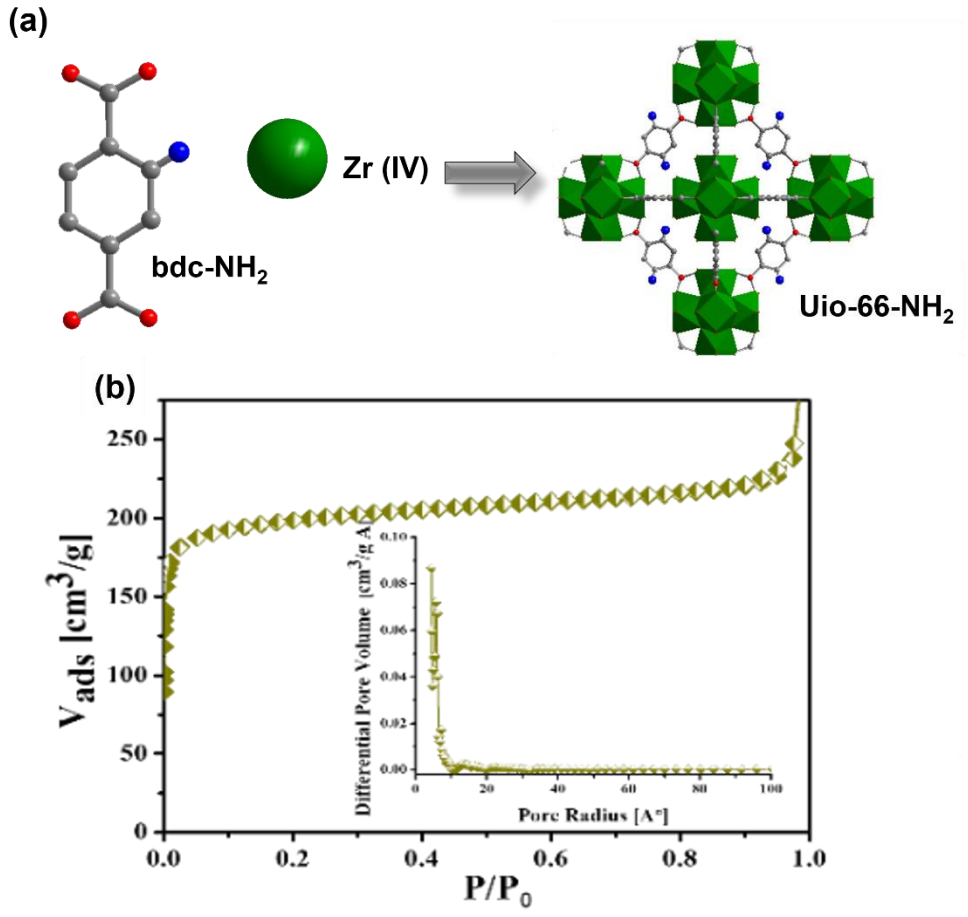

Figure S1. (a) Synthesis and 3D view of UiO-66-NH_2 (b) Nitrogen adsorption isotherm measured at 77 K of UiO-66-NH_2 inset shows micro pore distribution calculated via NLDFT method

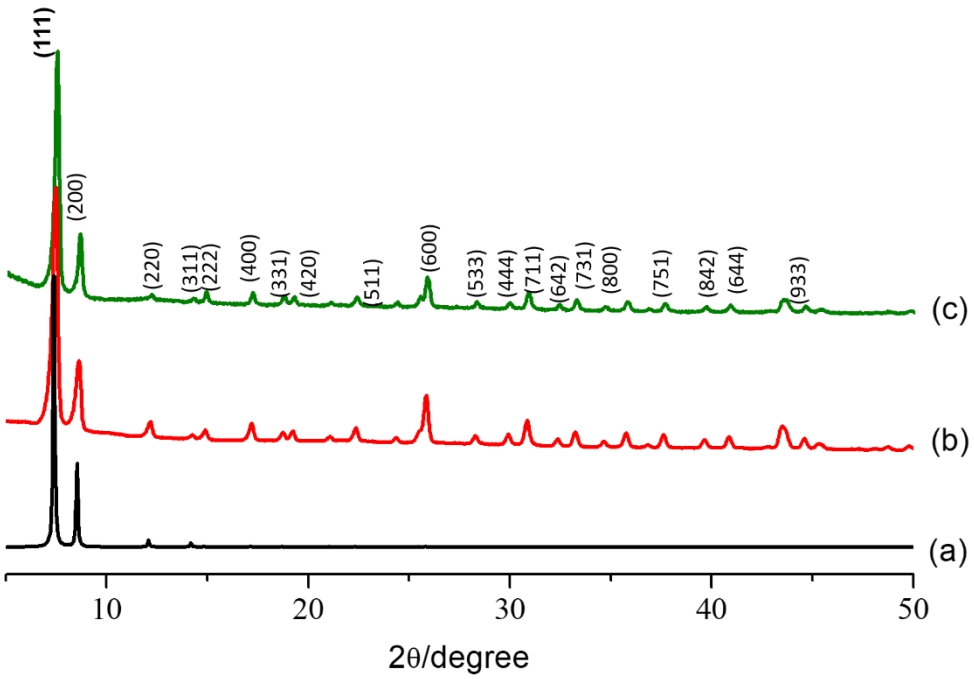

Figure S2. Powder XRD patterns of **UiO-66-NH_2** (simulated pattern (a, black), as-synthesized pattern (b, red) and pattern of sample activated at 160 $^{\circ}$C to remove synthesis solvent (c, green pattern).

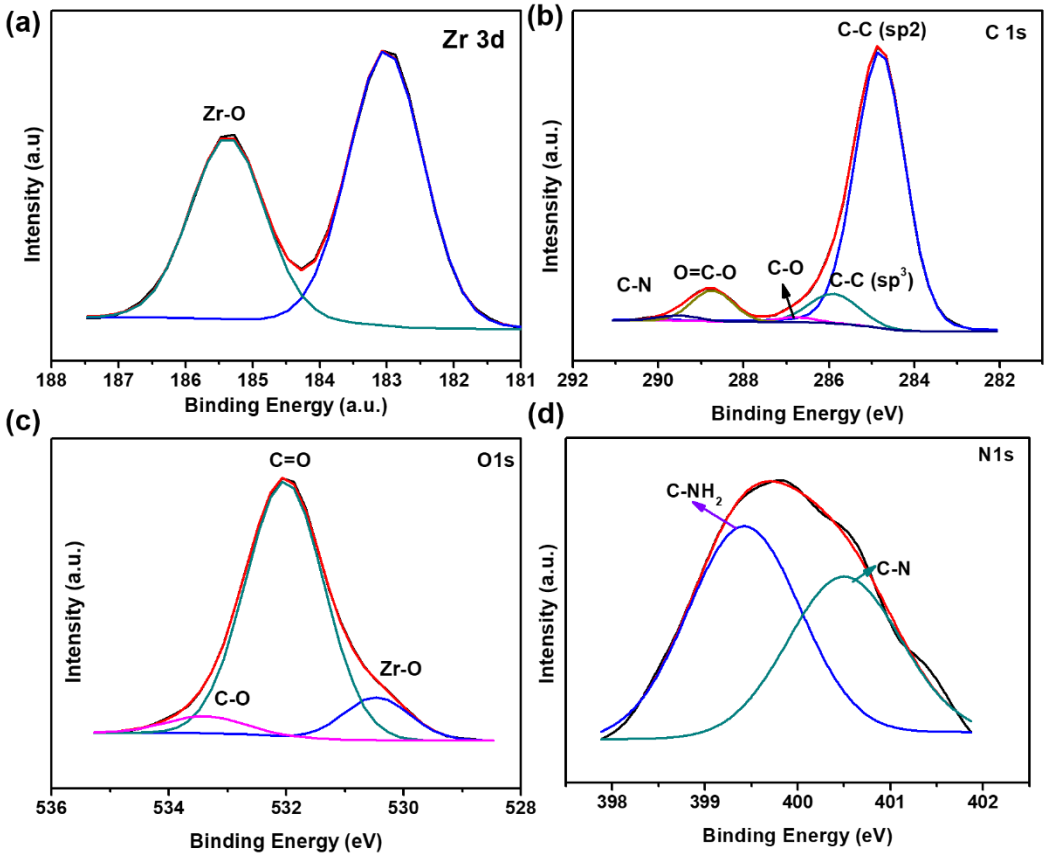

Figure S3. (a) High-resolution XPS spectra of UiO-66-NH_2 (a) Zr 3d (b) C1s, (c) O1s (d) N1s shows coordination environment between Zr metal ion with amino organic linker.

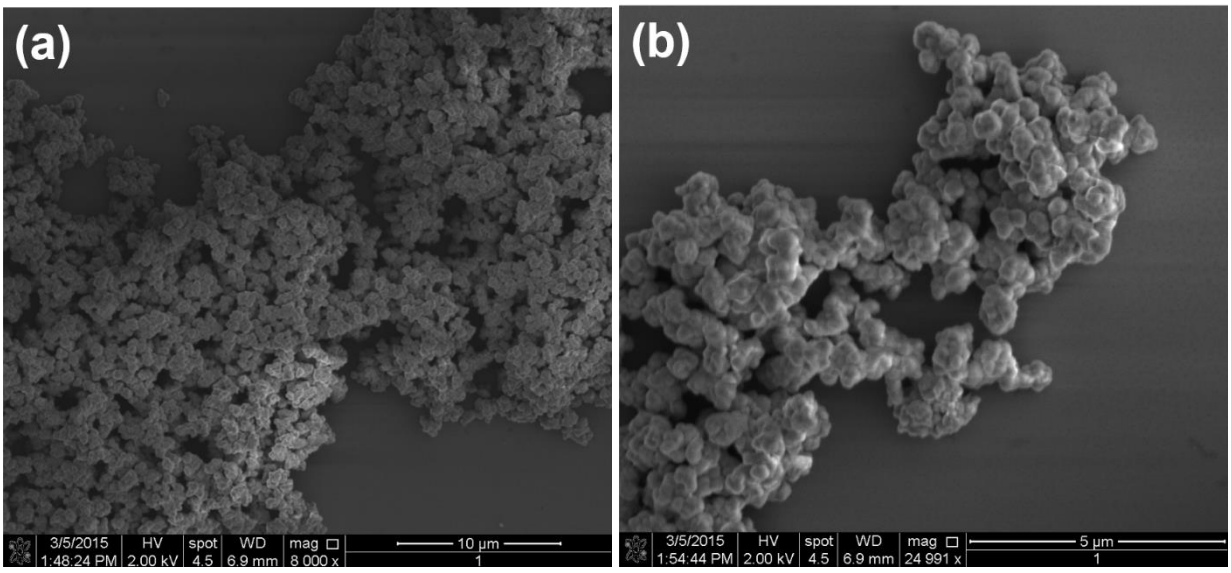

Figure S4. SEM micrographs (a, b) of UiO-66-NH_2 showing bundle of octahedron nanocrystals

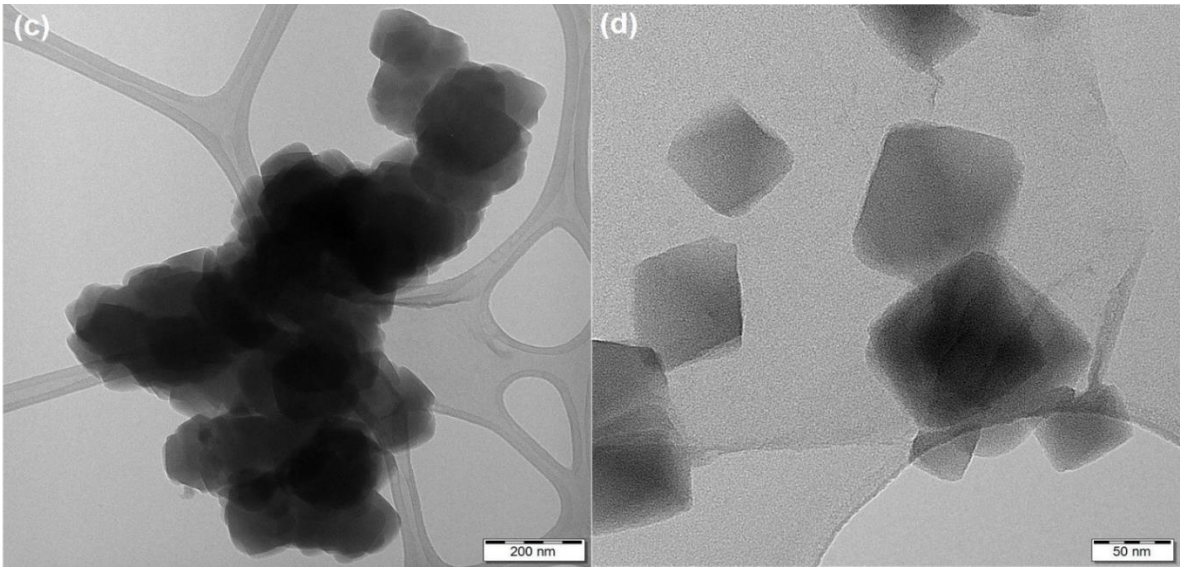

Figure S5. TEM micrographs (c, d) show octahedral nanocrystals and confirm a size of the crystals around 150-200 nm.

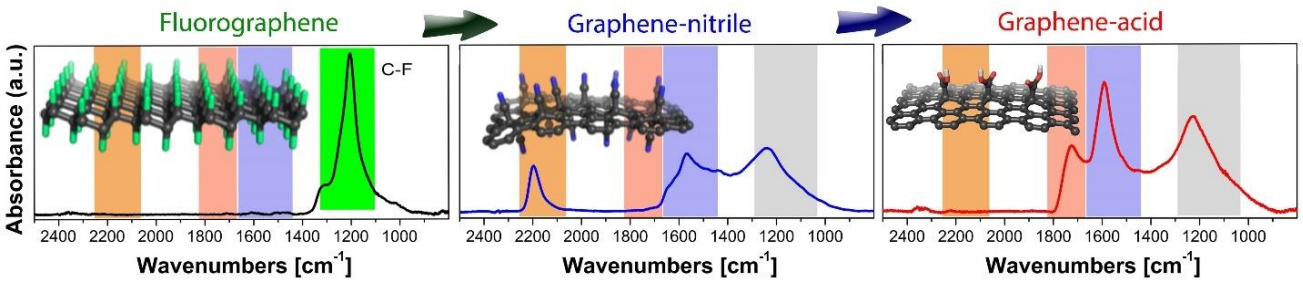

Figure S6. Schematic representation of synthesis of graphene acid from graphene nitrile and Fluorographene and the corresponding FT-IR spectra

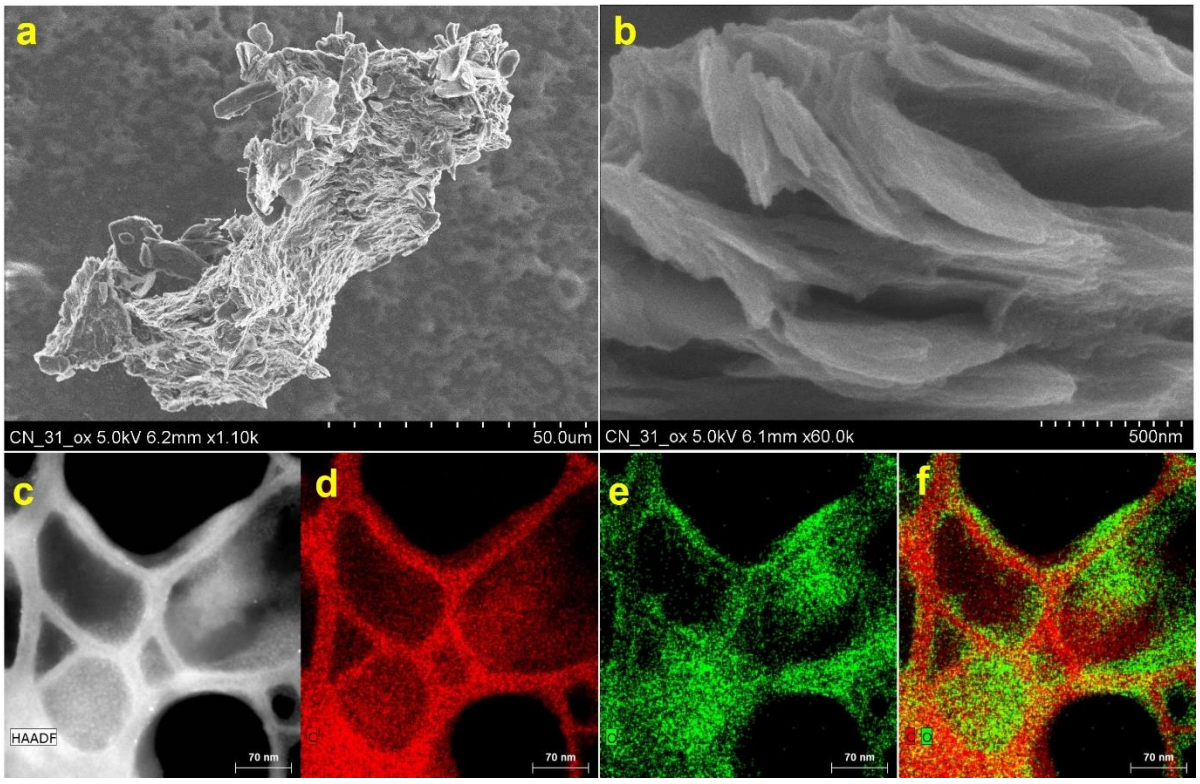

Figure S7a. (a-b) SEM micrographs of graphene acid showing evidence of the layered nature; EDS chemical mapping reveals homogeneous distribution of elements: (c) HAADF image, (d) carbon, (e) oxygen (f) carbon and oxygen elements distributed through layered structure.

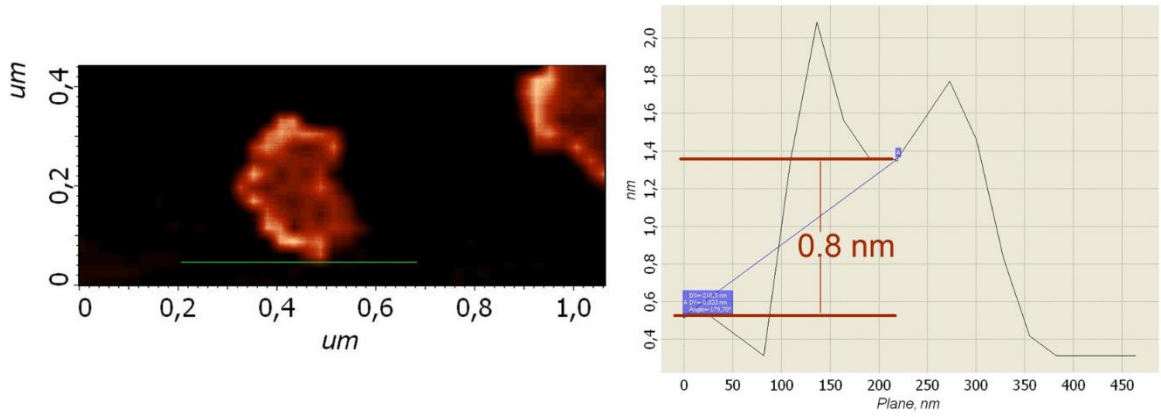

Figure S7b. (left) Atomic Force Microscopy (AFM) image of GA nanosheets (b) Height profile is showing 0.8 nm thickness.

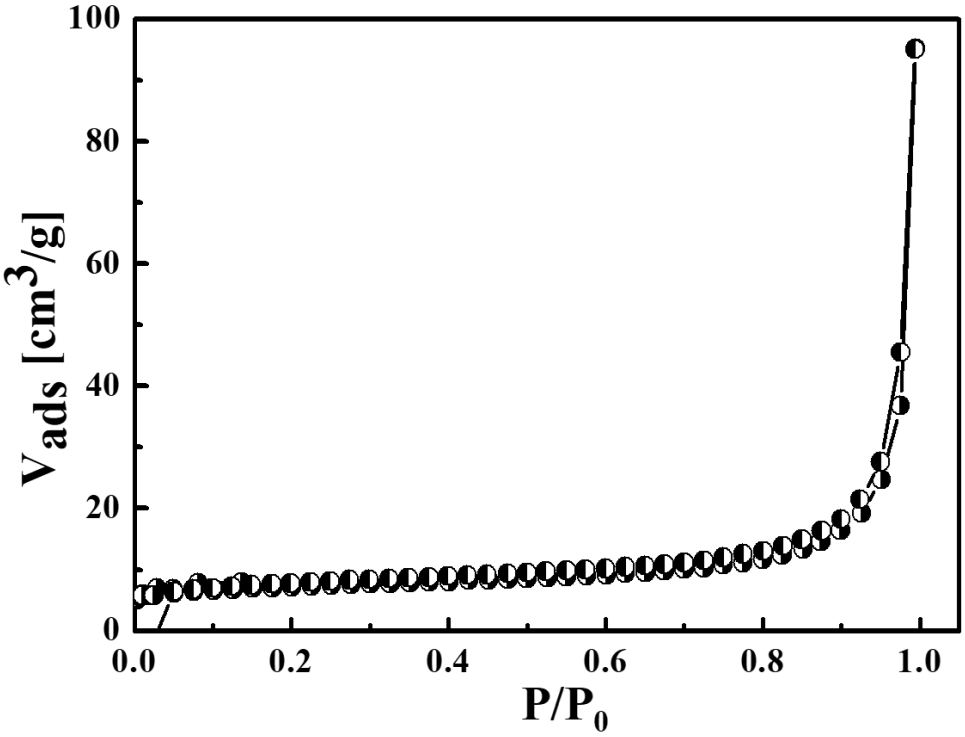

Figure S8. Nitrogen adsorption-desorption isotherm of pristine GA measured at 77 K shows typical type-II surface adsorption.

Figure S9. Photograph of black gel of **GA@UiO-66-NH_2**.

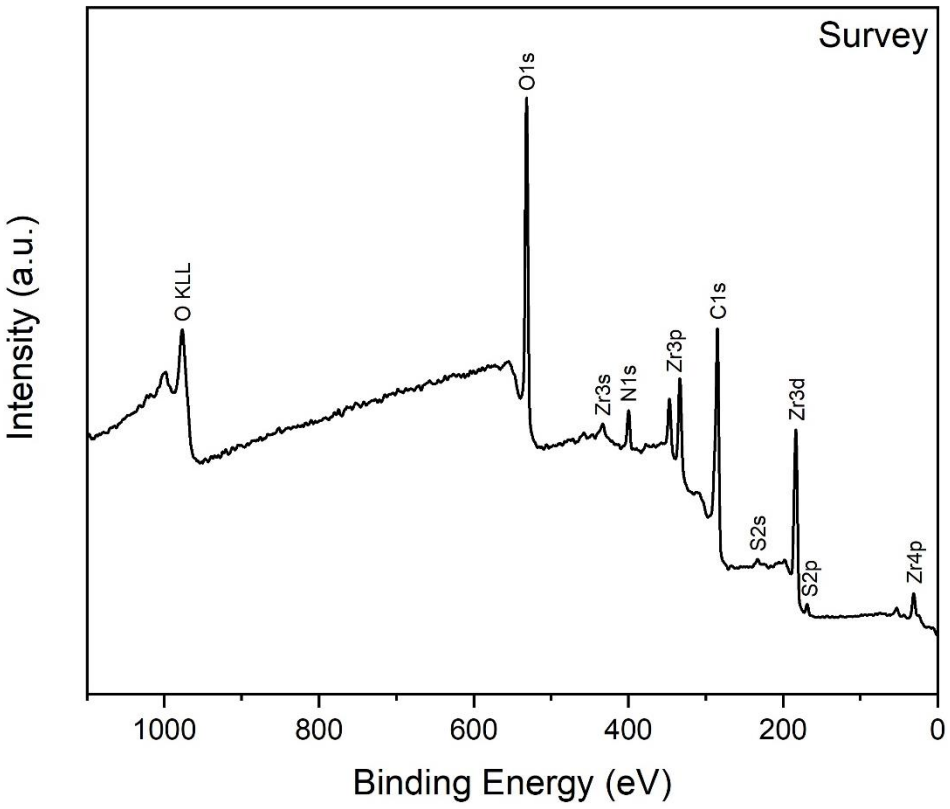

Figure S10a. XPS survey spectrum of **GA@UiO-66-NH_2** shows presence of zirconium, carbon, nitrogen and oxygen in the sample.

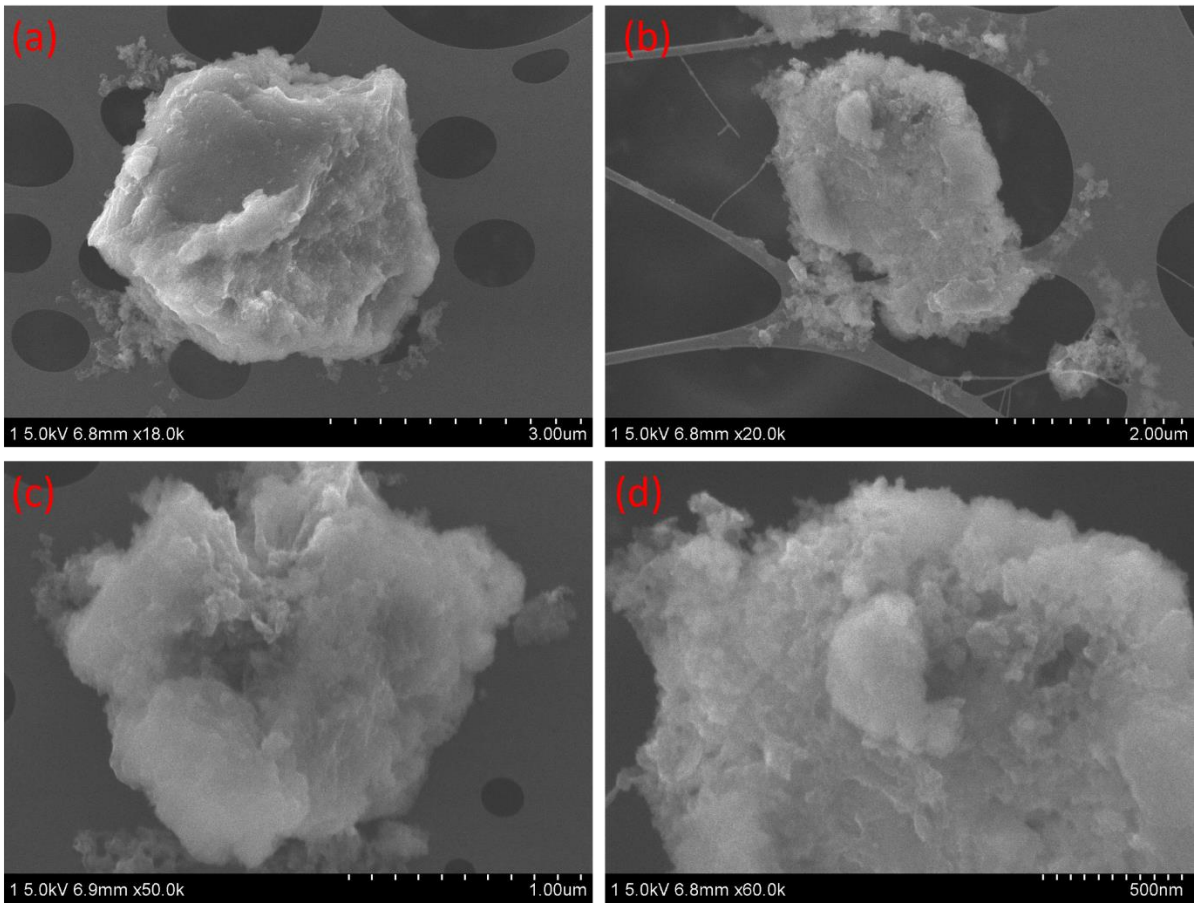

Figure S10b. FESEM (a-d) analysis of covalent **GA@UiO-66-NH_2** at different magnification showing homogeneous distribution of octahedron nanocrystals intercalated in between graphene acid layers.

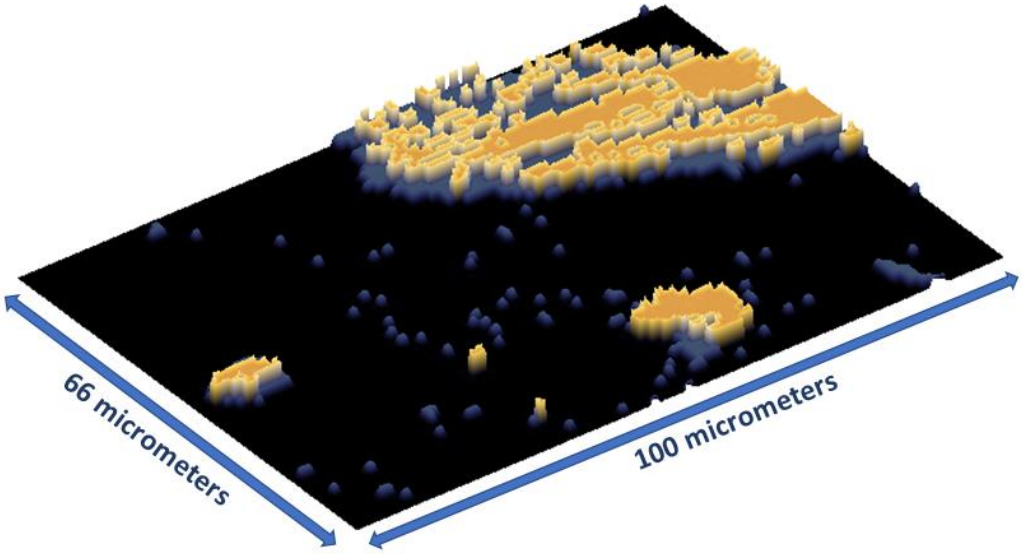

Figure S11. Map of the Raman intensity corresponding to amide groups (yellow region) of the hybrid across the sample.

Discussion:

The Raman spectrum of GA shows prominent peaks for the D-band (1330 cm^{-1}) and G-band (1595 cm^{-1}). The band ratio I_D/I_G = 1.34 is due to bonding disorders, and carboxylate functional groups located on the basal plane of GA (Fig 2d). The Raman spectrum of **GA@UiO-66-NH_2** after covalent attachment, shows two bands present at 1340 (D-band) and 1593 cm^{-1} (G-band) (Fig 2d), but the shape of the D and G bands of the hybrid differ substantially from GA. Additionally, Raman imaging was performed on a representative section of the **GA@UiO-66-NH_2** sample combined with a follow-up hierarchical cluster analysis via Ward's method. This unveiled two structural motifs which were later confirmed by spectral analysis of the measured data. The second motif, hybrid **GA@UiO-66-NH_2** can be interpreted as a combination of several vibration states: D-band, G-band and the underlying vibrations of C-N bonds, particularly Amide II and Amide III (above figure).[35] Further, The Raman map shows a spatial distribution of the intensity of the D-Band. The overall intensity of the D-band remains nearly unchanged over the scanned area. Next, the calculated map shows a spatial distribution of two found motifs detected on the surface of the measured nanomaterial. The first cluster represents pristine GA (blue color, 65 % of the surface) and the second cluster represents the amide functionalized motif (green color, 35 % of the

surface) . Therefore, both the Raman spectroscopy results successfully confirm the presence of amide bonds in **GA@UiO-66-NH_2**.

Table S1: Elemental Composition in at % of GA@Uio-66-NH2 and Uio-66-NH2 by XPS analysis

Compound	Zirconium	Carbon	Nitrogen	Oxygen
GA@Uio-66-NH_2	3.80	68.33	4.68	23.19
Uio-66-NH_2	3.52	72.16	3.37	20.95

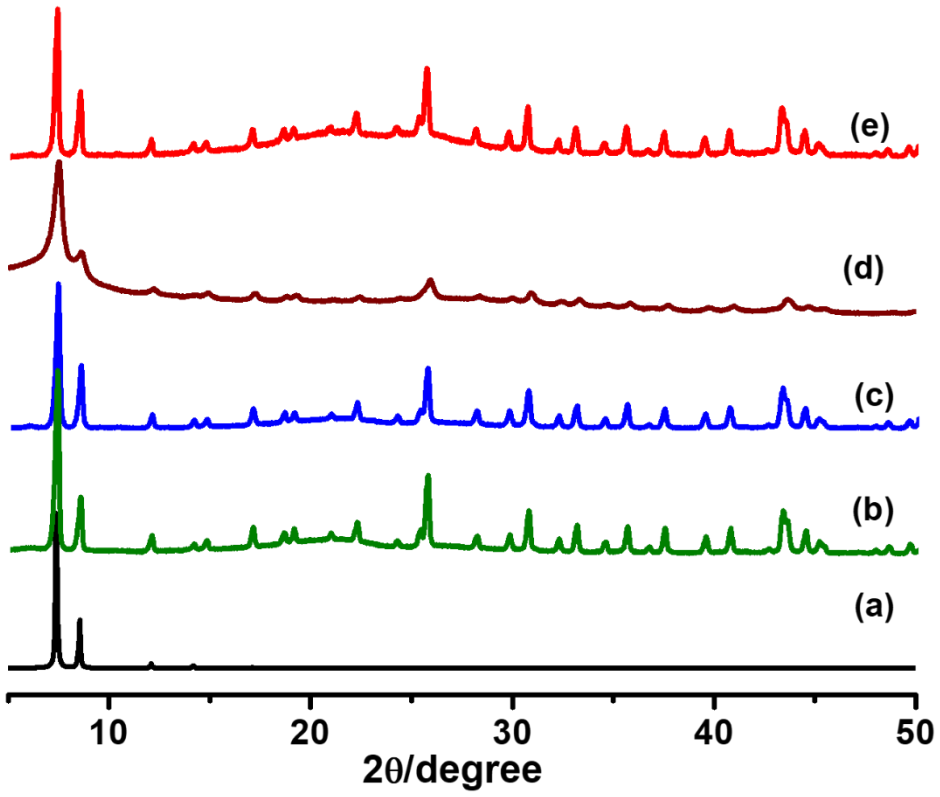

Figure S12. Powder XRD patterns of (a) UiO-66 (simulated), (b) UiO-66 (measured), (c) UiO-66-NH_2, (d) GA@UiO-66, and(e) a physical mixture of Uio-66-NH_2 and graphene acid (denoted as GA/Uio-66-NH_2) the powder XRD data shows phase purity and structural integrity of respective materials. The broader reflections found in sample (d) suggest nanosizing of the UiO-66-NH_2 crystals during intercalation.

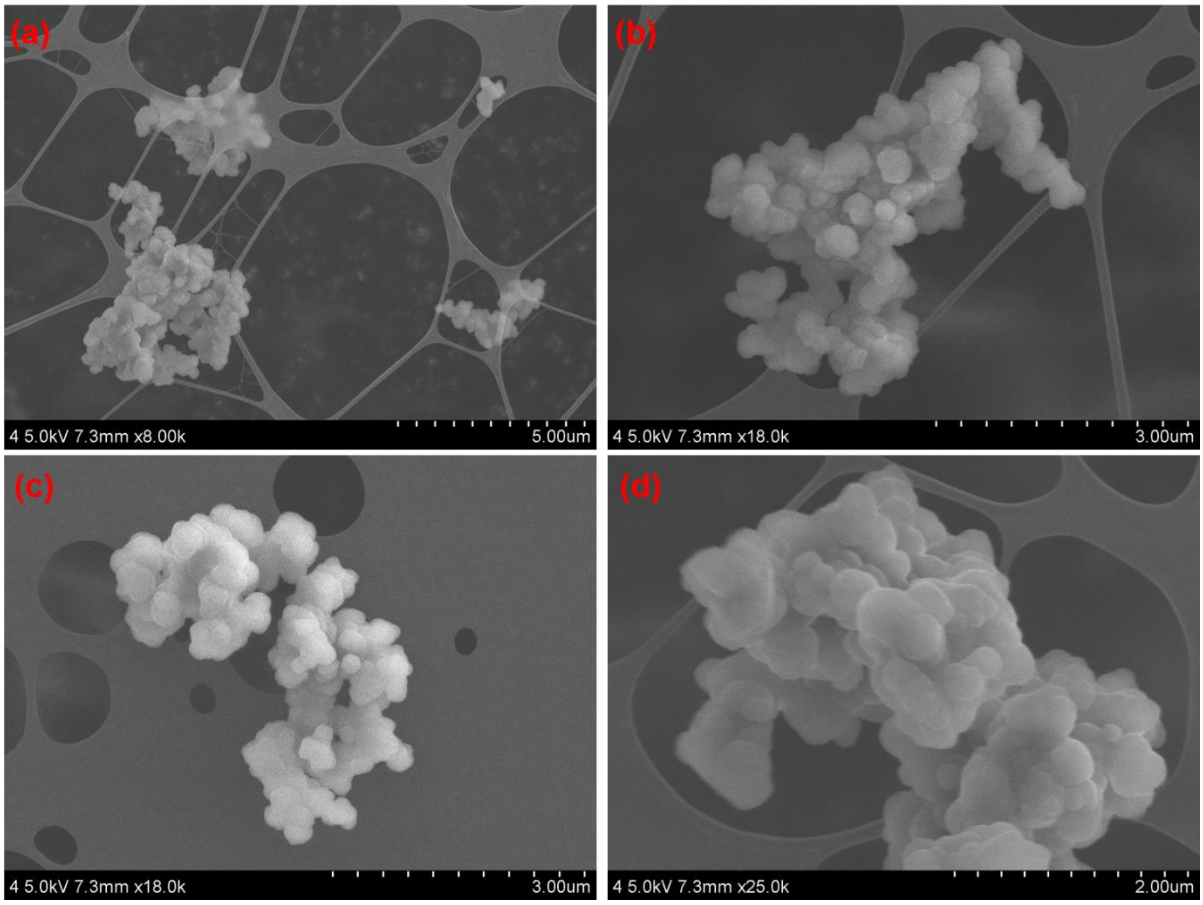

Figure S13. SEM micrographs at different magnifications (a, d) of UiO-66 showing bundle of octahedron nanocrystals, it clearly reveals size of pristine Uio-66 crystals around 200-300 nm

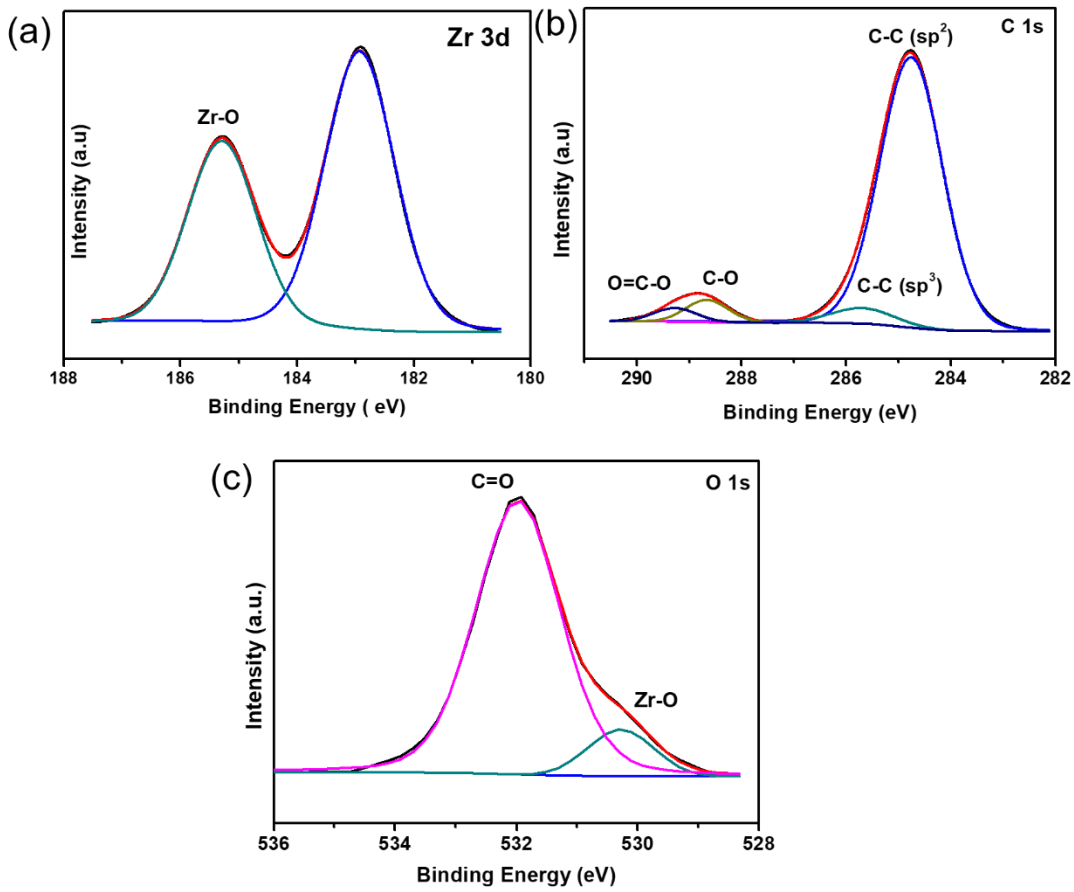

Figure S14 (a) High-resolution XPS spectra of **UiO-66** (a) Zr 3d (b) C1s, (c) O1s, shows coordination environment between Zr metal ion with benzene dicarboxylate organic linker.

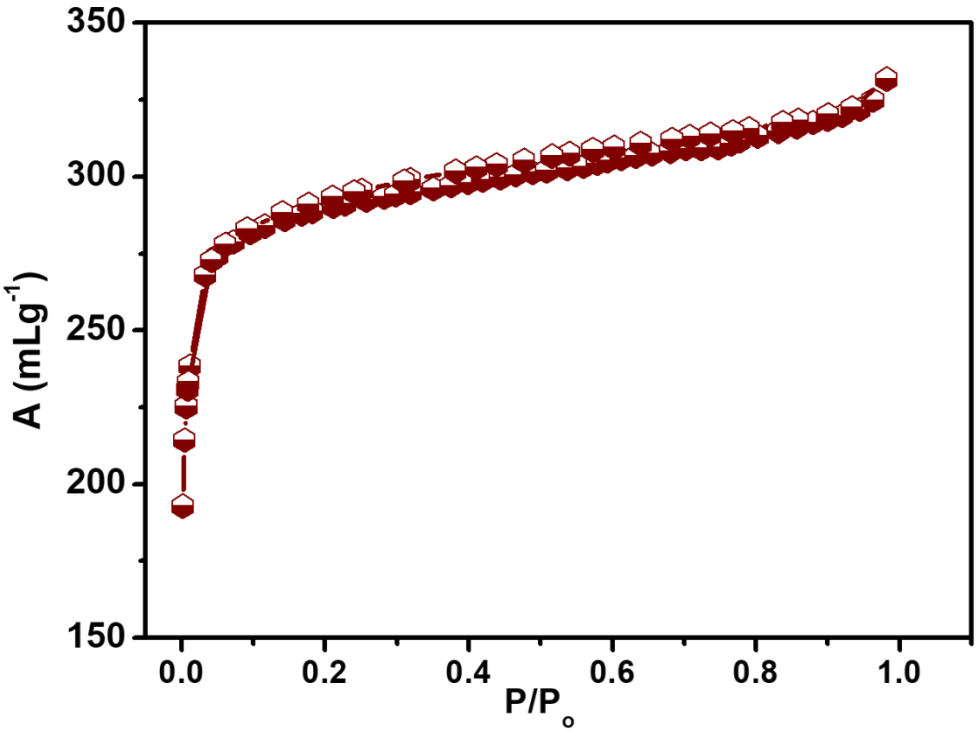

Figure S15 Nitrogen adsorption-desorption isotherm of UiO-66 measured at 77 K showing typical type-I microporous behavior.

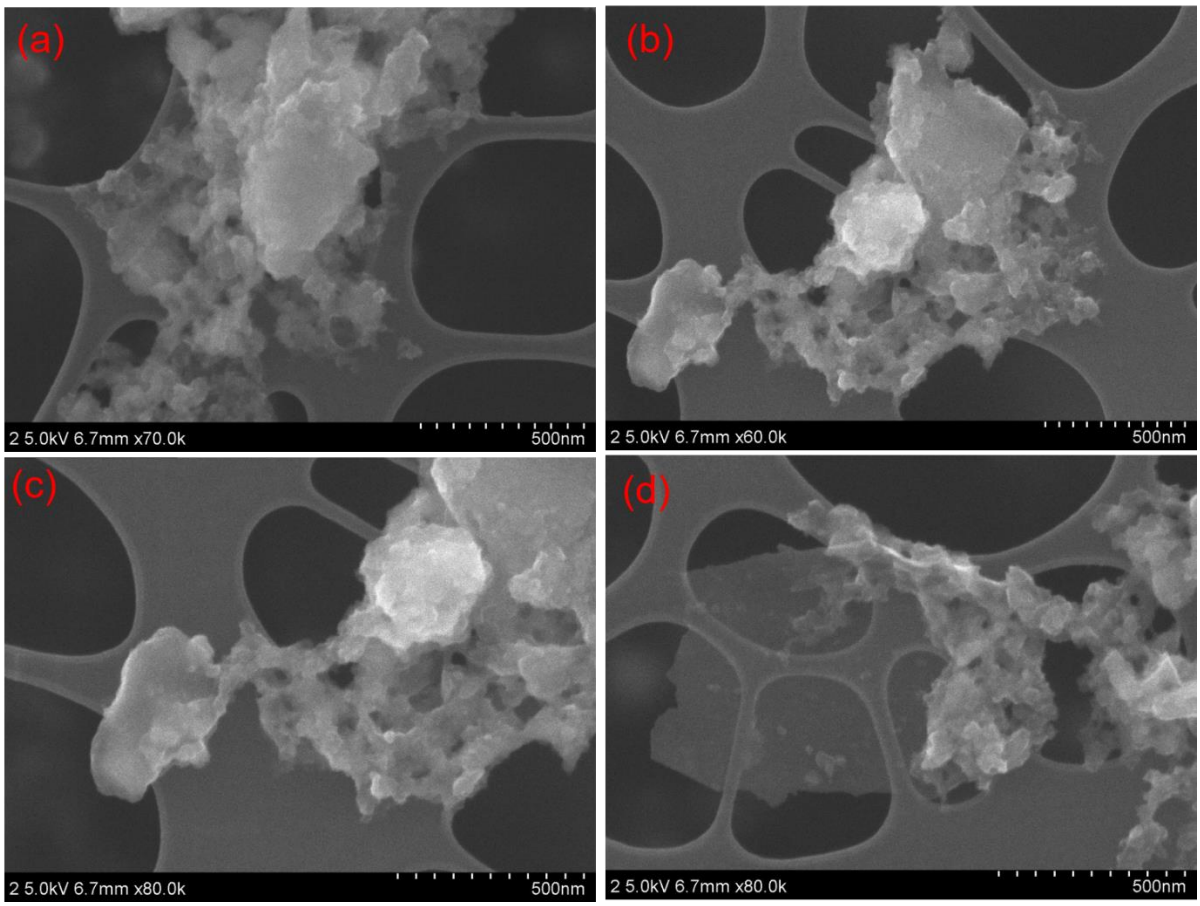

Figure S16 FE-SEM micrographs of **GA@UiO-66** (a-d) showing bundles of octahedron nanocrystals encapsulated in the graphene nanosheets.

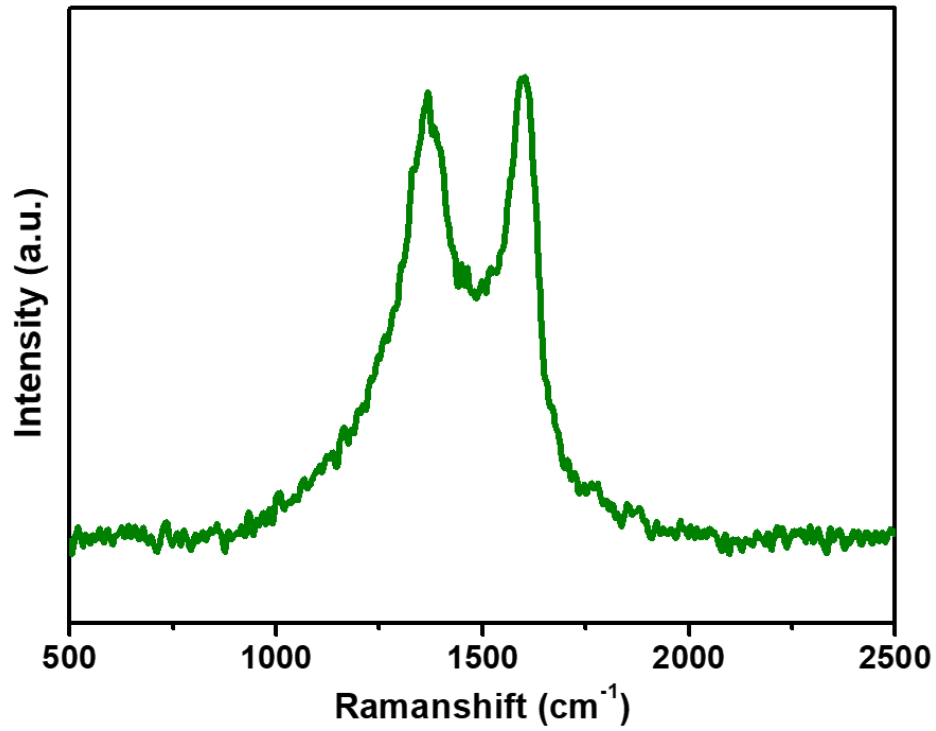

Figure S17. Raman spectrum of **GA@Uio-66** reveals its D and G band, respectively.

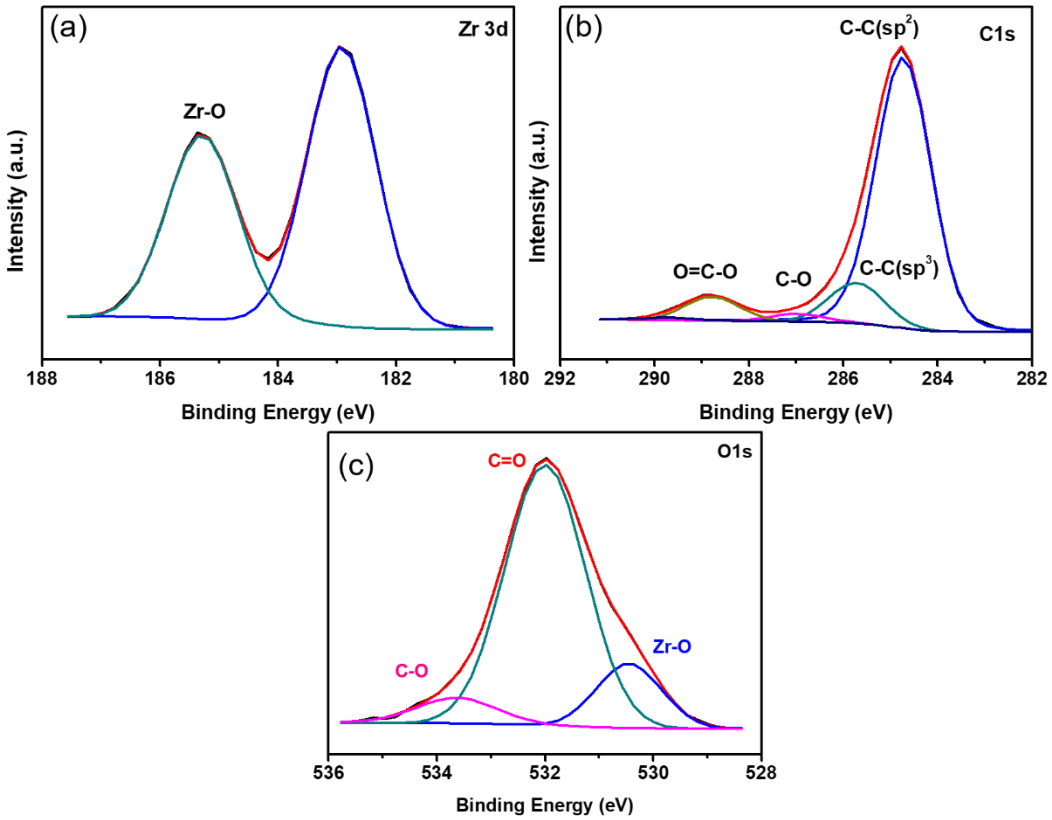

Figure S18. (a) High-resolution XPS spectra of **GA@UiO-66** (a) Zr 3d (b) C1s, (c) O1s, shows coordination environment between Zr metal ion with benzene dicarboxylate organic linker.

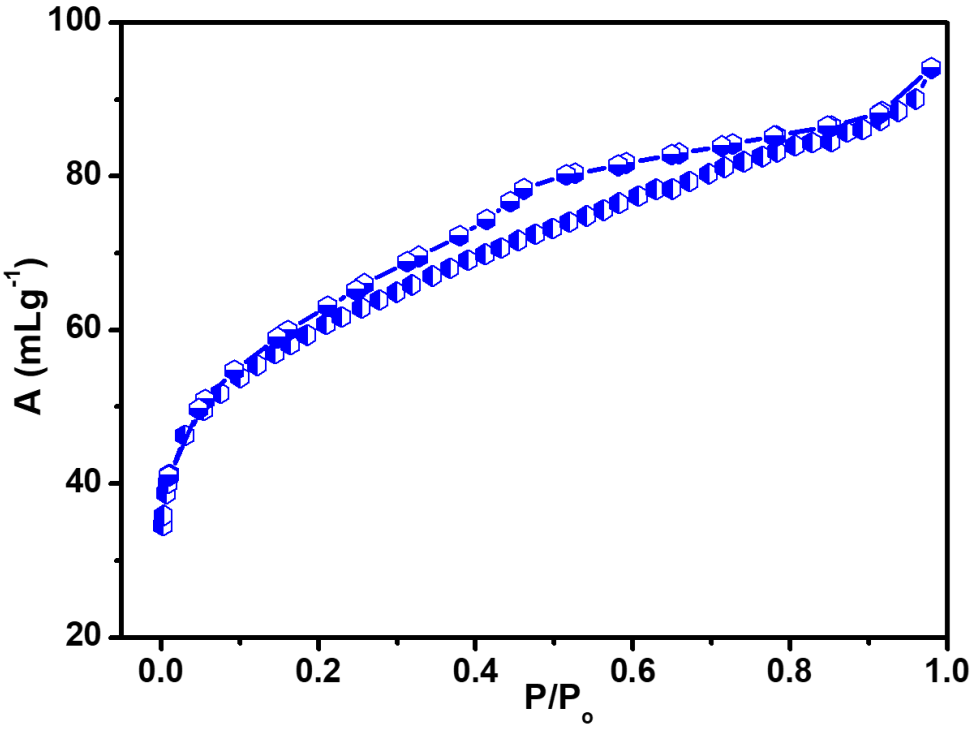

Figure S19. Nitrogen adsorption-desorption isotherm of **GA@UiO-66** measured at 77 K showing typical type-IV reveals micro-meso porous behavior with a hysteresis loop. Interestingly, it should be noted that the resultant hysterics clearly reveals existence of non-ordered pores, caused by noncovalent interaction between graphene acid layers with UiO-66 nanocrystals.

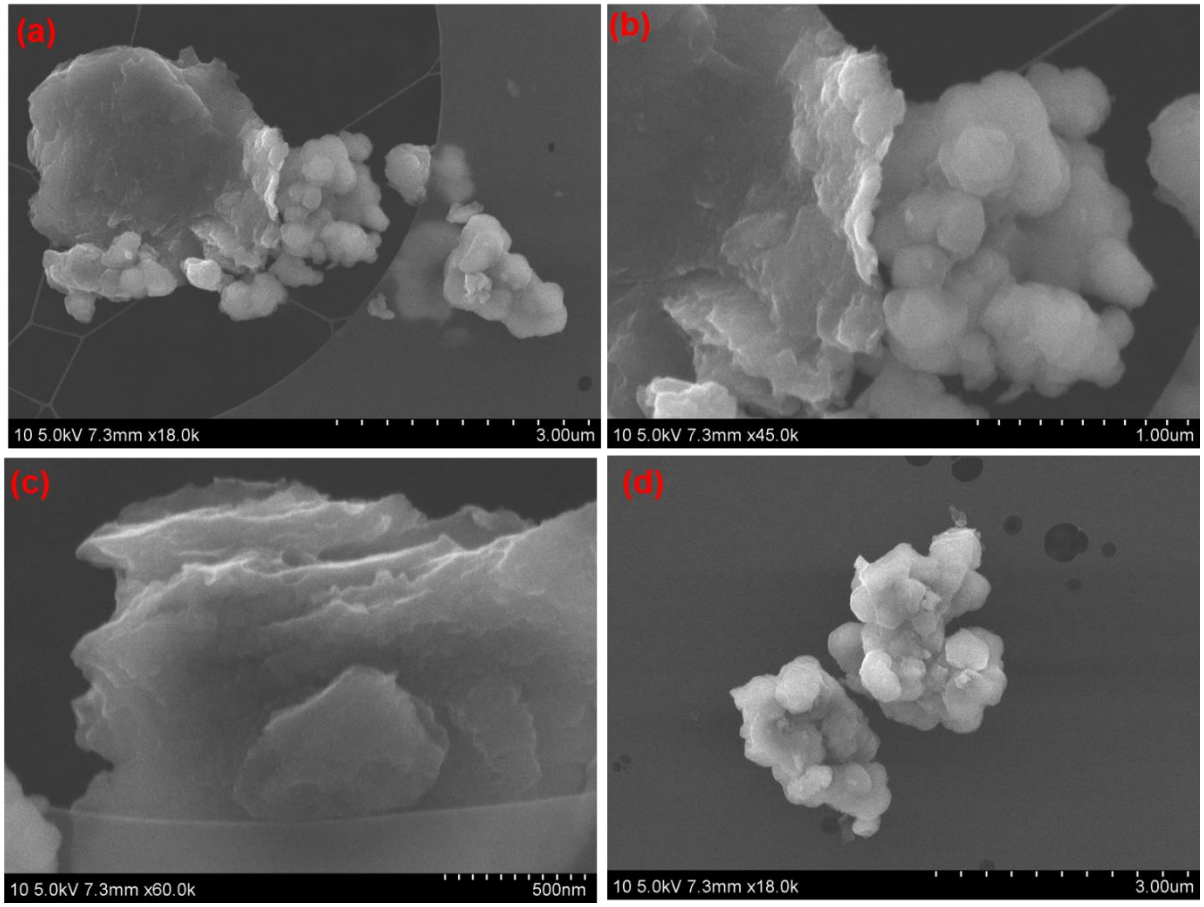

Figure S20. FE-SEM micrographs (a-d) of a physical mixture of GA and UiO-66-NH_2 at different magnifications, clearly shows individual GA nanosheets and micro octahedron crystals.

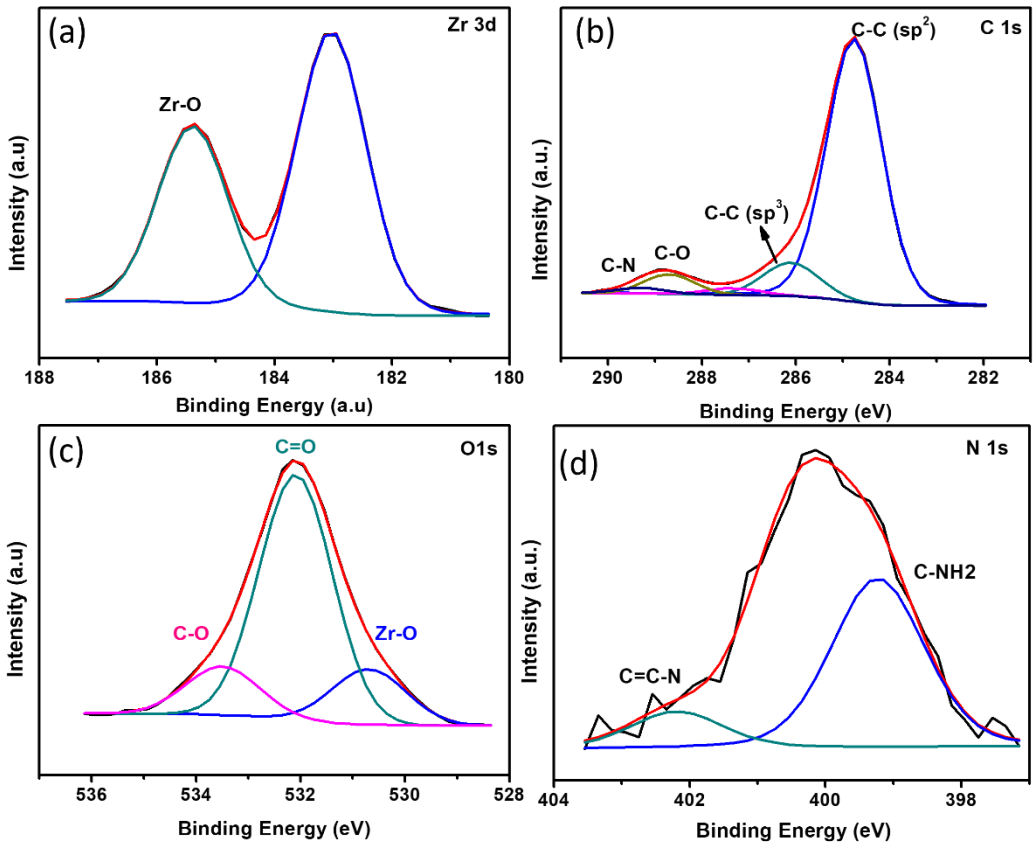

Figure S21 (a) High-resolution XPS spectra of physical mixture of a GA and UiO-66-NH_2 (a) Zr 3d (b) C1s, (c) O1s, shows coordination environment between Zr metal ion with benzene dicarboxylate organic linker. The XPS data of N1s of the physical mixture of GA/UiO-66-NH_2 does not feature the peak corresponding to the amide bond between UiO-66 nanocrystals and graphene nanosheets in contrast to GA@UiO-66-NH_2.

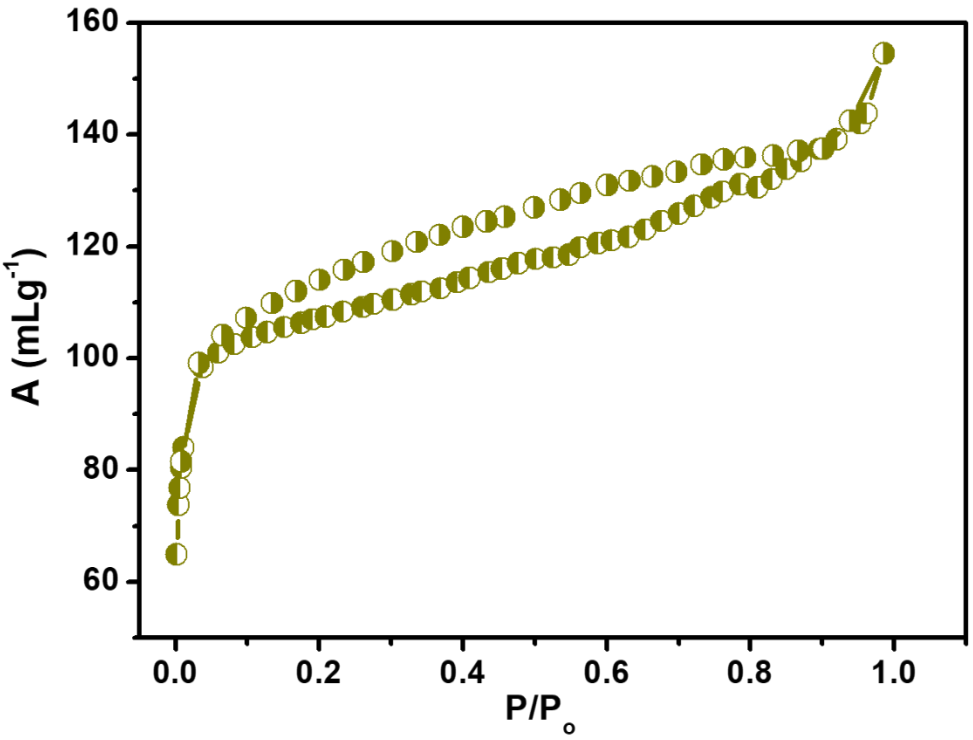

Figure S22 Nitrogen adsorption isotherm of a physical mixture of GA and UiO-66-NH_2 nanocrystals measured at 77 K, it shows typical type-IV isotherm with both meso and micro pores. The obtained hysteresis clearly reveals irregular meso pores originated from defects of graphene acid layers during grinding and micro pores originated from UiO-66-NH_2 nanocrystals.

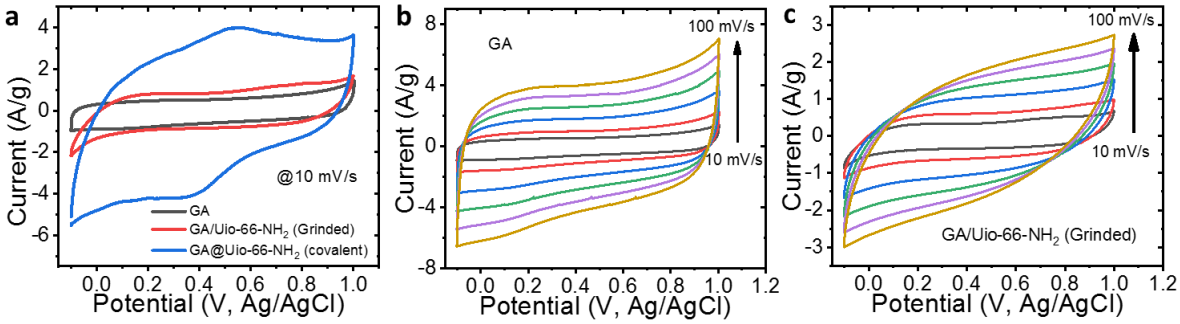

Figure S23 (a) cyclic voltammetry curves for GA, covalent **GA@UiO-66-NH_2** and grinded **GA/UiO-66-NH_2** electrodes at 10 mV/s. (b, c) CV curves for GA and grinded **GA@UiO-66-NH_2** electrodes recorded at various scan rates, respectively.

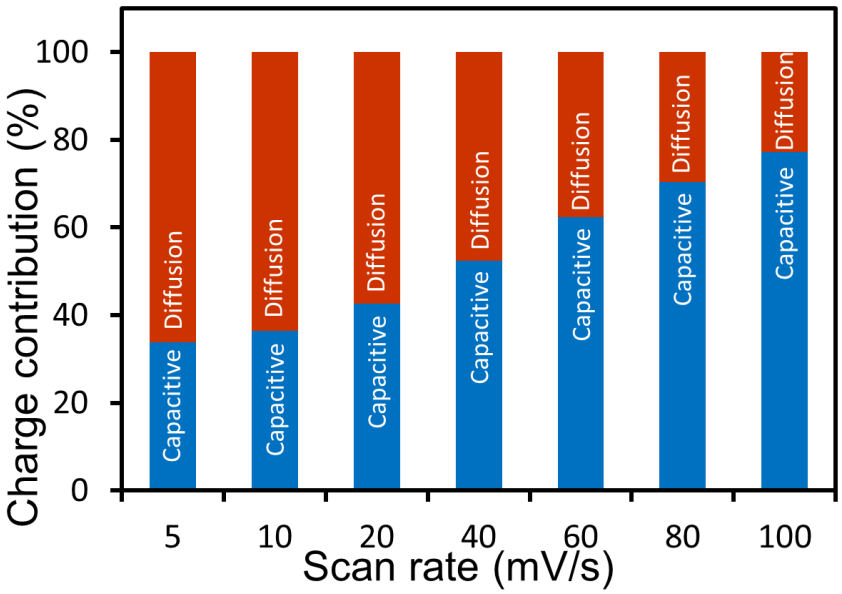

Figure S24. Variation of charge contributions in total current with scan rate for **GA@UiO-66-NH$_2$** hybrid electrode, suggesting successive increase in the capacitive contribution with scan rates.

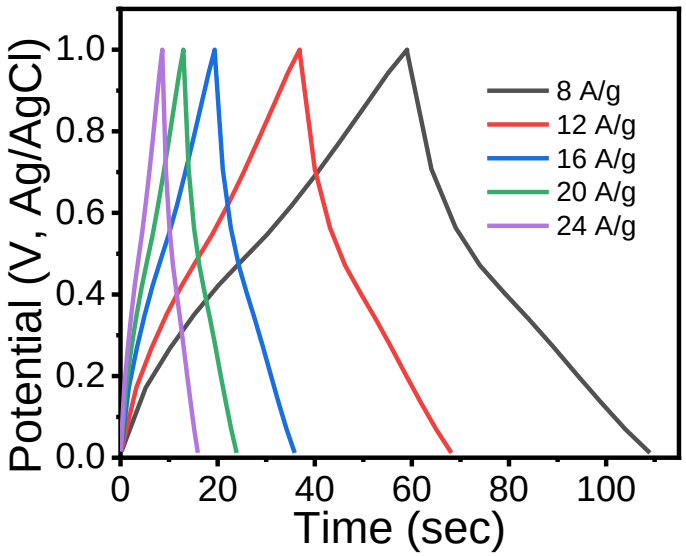

Figure S25. Charge/discharge curves for **GA@UiO-66-NH$_2$** hybrid electrode recorded at very high current densities.

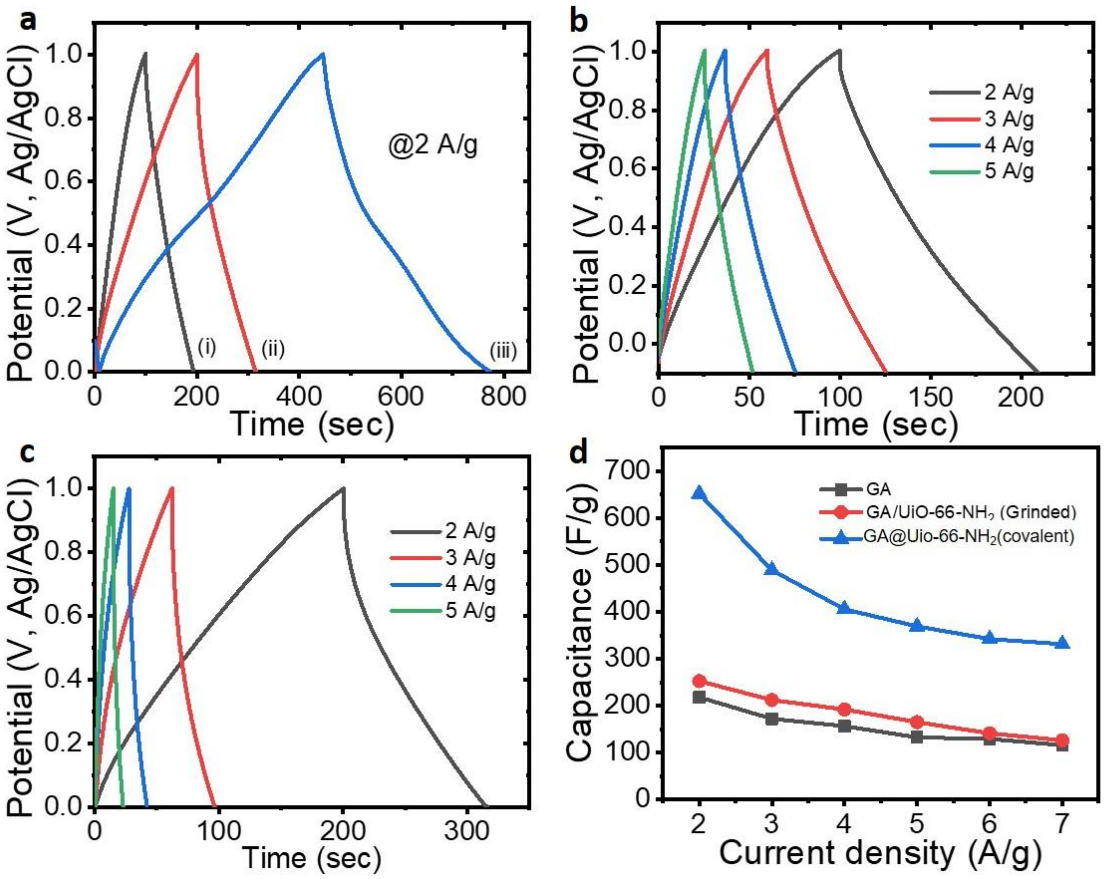

Figure S26 (a) Charge/discharge curves for GA, covalent **GA@UiO-66-NH$_2$** and grinded **GA/UiO-66-NH$_2$** electrodes at 2 A/g. (b, c) CD curves for GA and grinded **GA/UiO-66-NH$_2$** electrodes at different current densities, respectively. (d) Variation of specific capacitance as a function of current density for GA, covalent **GA@UiO-66-NH$_2$** and grinded **GA/UiO-66-NH$_2$** electrodes.

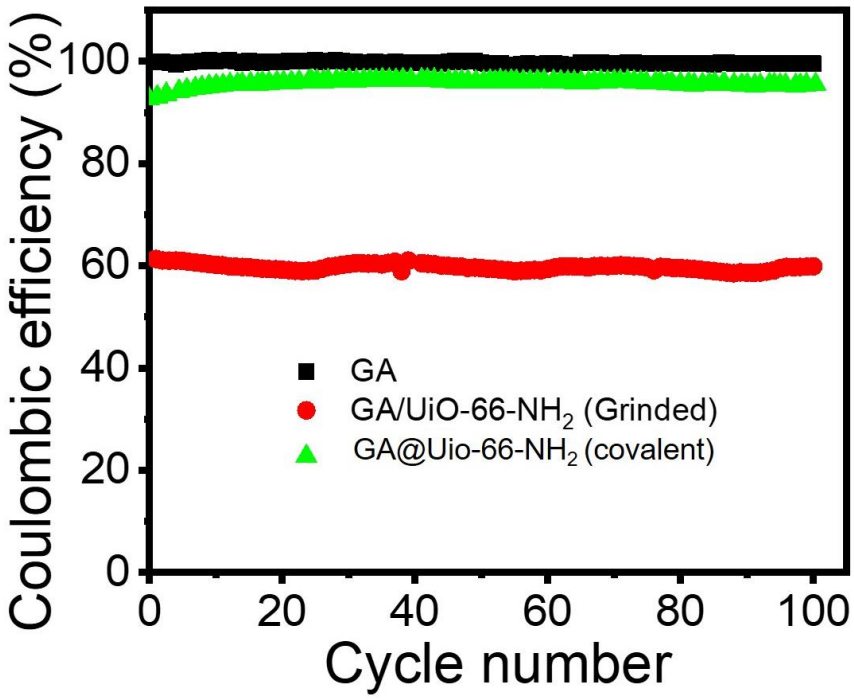

Figure S27 Coulombic efficiency for GA, covalent **GA@UiO-66-NH$_2$** and grinded **GA/UiO-66-NH$_2$** electrodes measured using galvanostatic charge/discharge curves at 3 A/g.

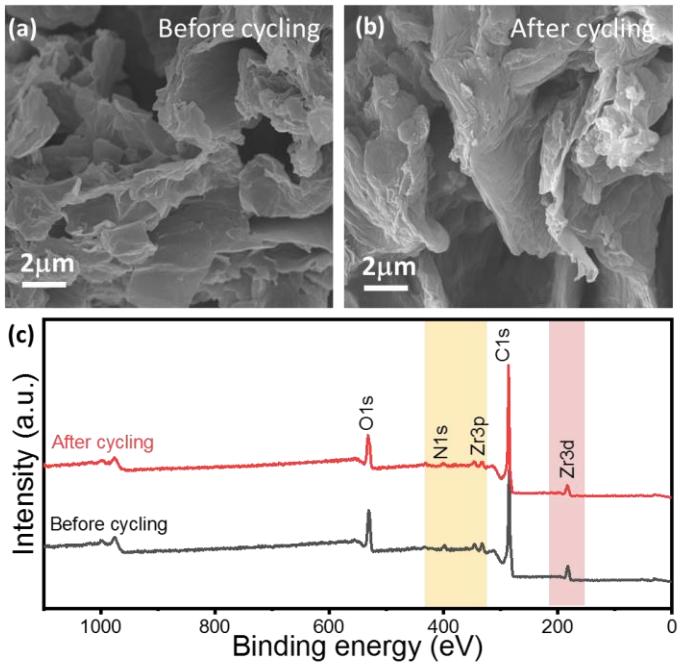

Figure S28 (a, b) SEM images of covalent **GA@UiO-66-NH_2** electrode, (c) Survey spectra of **GA@UiO-66-NH_2** electrodes before and after (20,000) charge/discharge cycles.

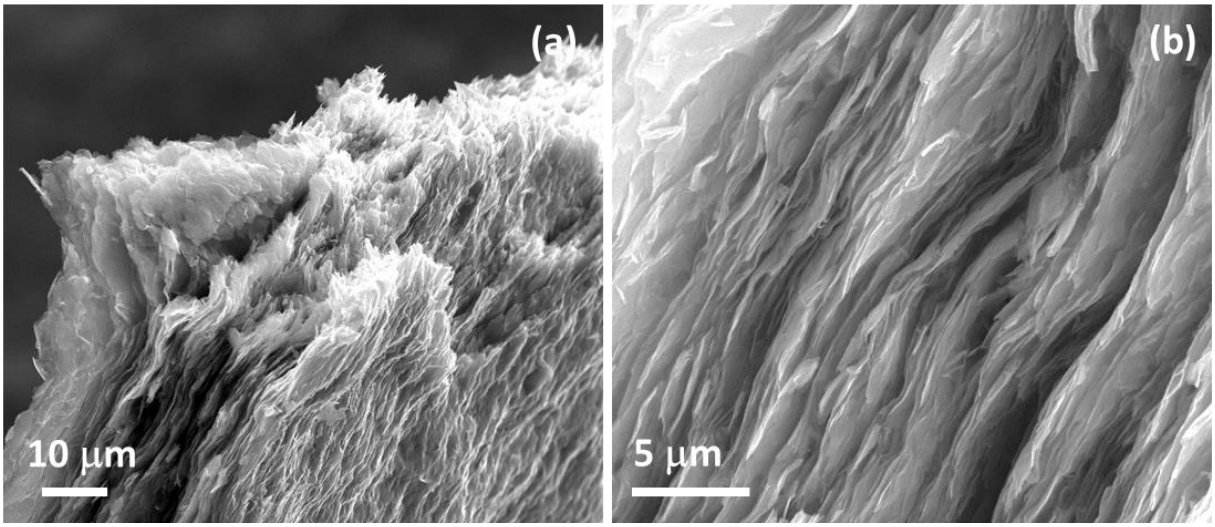

Figure S29 (a, b) Scanning electron micrograph and (c, d) Transmission electron micrograph images of $Ti_3C_2T_x$ samples. The surface morphological analysis shows the formation of few layered $Ti_3C_2T_x$ nanosheets.

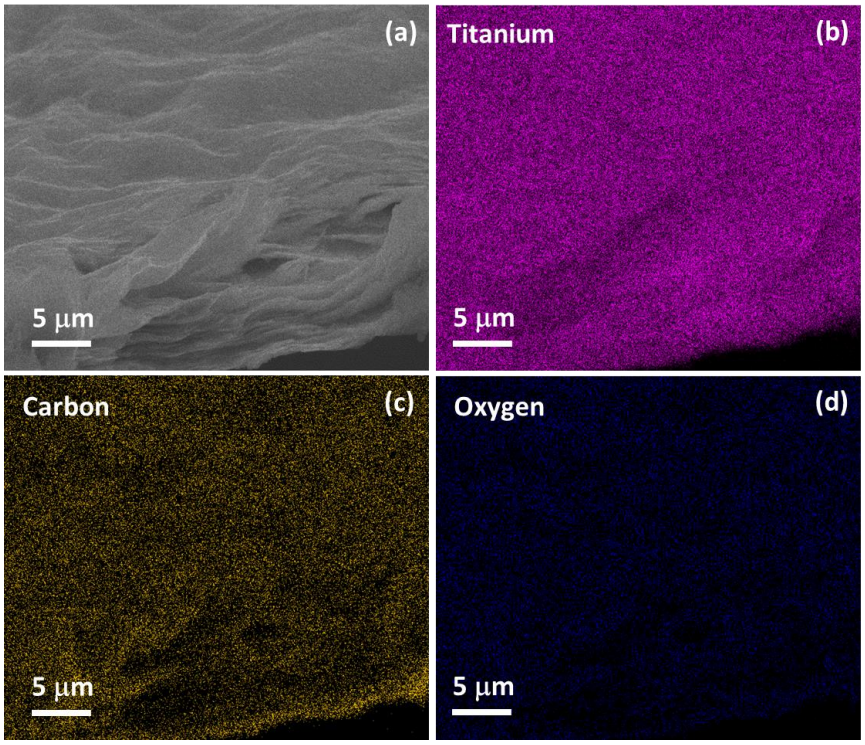

Figure S30. SEM-EDAX mapping of $Ti_3C_2T_x$ samples, which confirms the presence of Ti, C and O elements thereby confirming the formation of $Ti_3C_2T_x$ nanosheets.

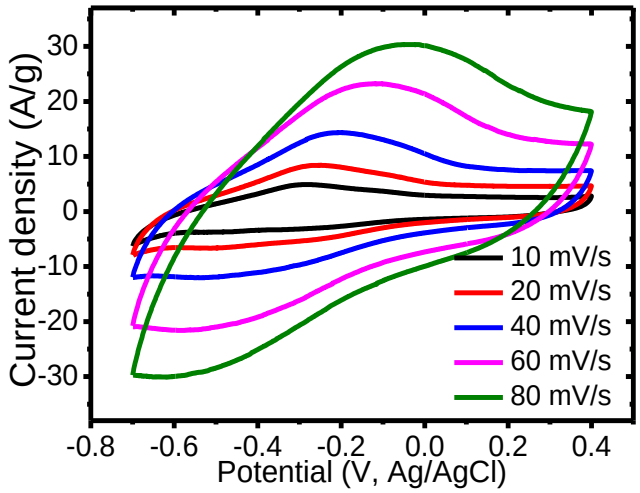

Figure S31. Cyclic voltammetry curves of $Ti_3C_2T_x$ coated on CF substrates measured at different scanning rates. The shapes of the curves demonstrates the pseudo-capacitive charge storage mechanism.

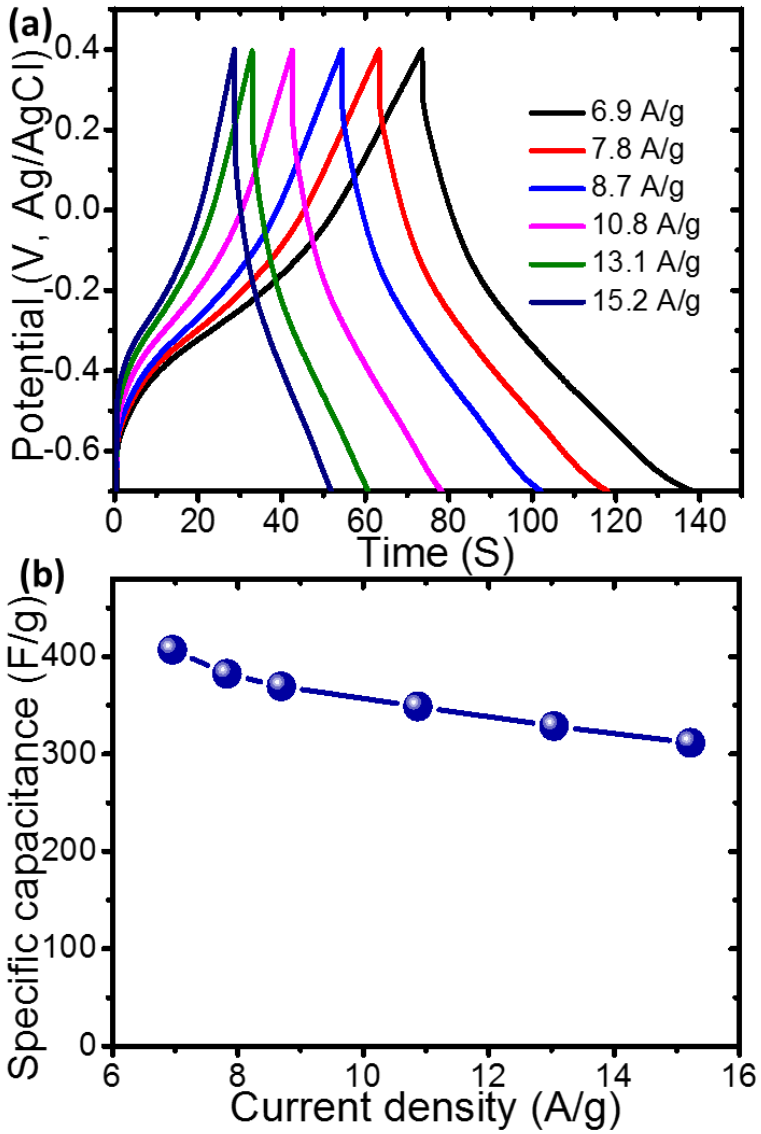

Figure S32. (a) Galvanostatic charge/discharge curves for $Ti_3C_2T_x$ coated on CF substrates recorded at different current densities. The shapes of GCD curves are not ideal triangular, suggesting the pseudo-capacitive contribution and support CV results. (b) Variation of specific capacitance with applied current density. The maximum specific capacitance was determined to be 406 F/g at 6.9 A/g, which was maintained to be 311 F/g at 15.2 A/g, suggesting 76% capacitance retention at high current densities.

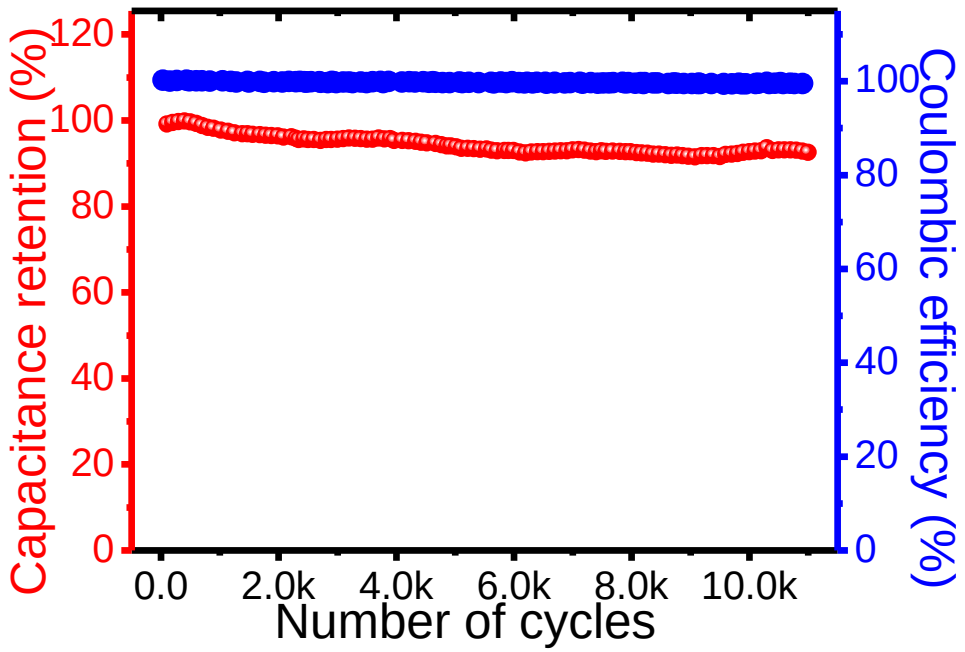

Figure S33. Long-term cycling stability of $Ti_3C_2T_x$ electrode measured at 10.8 A/g over 12,000 cycles. Notably, the electrode retained around 90% of the initial specific capacitance with almost 100% Coulombic efficiency after 12k cycles, suggesting excellent reversibility and structural stability of the material.

Table S2 Comparison of electrochemical performances of functionalized graphene in terms of specific capacitance and cycling stability.

Materials	Capacitance	Cycling stability	Reference
GA@UiO-66-NH_2	651 F/g @ 2A/g	94% over 20,000 cycles at 5 A/g	Present work
Fluorographene / 5-aminoisophthalic acid (Fg/Niso)	391 F/g @ 0.25 A/g	-	*Chem. Mater. 2019, 31, 4698−4709*
Bis-(phthalimidoethyl)-amine functionalized graphene oxide (GO-bis(PIEA))	287 F/g @ 1A/g	94.5 over 1000 cycles at 1000 mV/s	*Materials Chemistry and Physics 2019, 222, 45–54*
Dibenzylamine (DBA)-	205 F/g @ 1 mA/cm^2	No loss after 1000	*RSC Adv., 2018, 8, 6136–*

GO		cycles at 1 mA/cm^2	*6145*
p-phenylenediamine (PPD)-GO	174 F/g @ 1 mA/cmm^2	No loss after 1000 cycles at 1 mA/cm^2	*RSC Adv., 2018, 8, 6136–6145*
Diisopropylamine (DPA)-GO	260 F/g @ 1 mA/cmm^2	No loss after 1000 cycles at 1 mA/cm^2	*RSC Adv., 2018, 8, 6136–6145*
Piperidine (PA)-GO	290 F/g @ 1 mA/cmm^2	No loss after 1000 cycles at 1 mA/cm^2	*RSC Adv., 2018, 8, 6136–6145*
Graphene (PANI–G) hybrid with amide groups	623.1 F/g @ 0.3 A/g	510 F/g @ 50 A/g over 1000 cycles	*J. Phys. Chem. C 2012, 116, 37, 19699–19708*
Poly(o-methoxyaniline) nanocomposites with amine-functionalization of GO (POMA/f-GO)	422 F/g @ 0.5 A/g	95.2 % over 1000 cycles at 2 A/g	*J Mater Sci: Mater Electron, 2017, 28, 5776–5787*
Ethylene diamine (EDA) -rGO	119 F/g @ 2 mV/s	92.5 % over 10,000 cycles	*Nano Energy 2017, 31, 183–193*
Butane-1,4-diamine (BDA)-rGO	134 F/g @ 10 mV/s	93.2 % over 10,000 cycles	*Nano Energy 2017, 31, 183–193*
Tris(2-aminoethyl) amine (Tris) -rGO	131 F/g @ 2 mV/s	95.6% over 10,000	*Nano Energy 2017, 31, 183–193*
Carboxyl-functionalized GO-polyaniline	525 F/g @ 0.3 A/g	87% over 200 cycles at 1 A/g	*J. Mater. Chem., 2012, 22, 13619-13624*
Amine functionalized graphene oxide (FGO)-poly ortho aminophenol (POAP) FGO-235/POAP	820 C/g	-	*Electrochimica Acta 2018, 292, 789-804*
Amine functionalized graphene oxide (FGO)-poly ortho aminophenol (POAP) FGO-178/POAP	348 C/g	-	*Electrochimica Acta 2018, 292, 789-804*
Polyaniline-graphene (PANI−G) with amide groups	623.1 F/g @ 0.3 A/g	No significant loss after 500 cycles at 50 A/g	*J. Phys. Chem. C 2012, 116, 19699*